Title
THE FIRST H-BAND SPECTRUM OF THE GIANT PLANET β PICTORIS b

Journal
The Astrophysical Journal Letters, 798(1)

ISSN
2041-8205

Authors
Chilcote, Jeffrey
Barman, Travis
Fitzgerald, Michael P
et al.

Publication Date
2015

DOI
10.1088/2041-8205/798/1/l3

Peer reviewed

The Astrophysical Journal Letters, 798:L3 (5pp), 2015 January 1 doi:10.1088/2041-8205/798/1/L3

THE FIRST *H*-BAND SPECTRUM OF THE GIANT PLANET β PICTORIS b

Jeffrey Chilcote[1,2], Travis Barman[3], Michael P. Fitzgerald[1], James R. Graham[4], James E. Larkin[1], Bruce Macintosh[5,6], Brian Bauman[6], Adam S. Burrows[7], Andrew Cardwell[8], Robert J. De Rosa[9,10], Daren Dillon[11], René Doyon[12], Jennifer Dunn[13], Darren Erikson[13], Donald Gavel[11], Stephen J. Goodsell[14], Markus Hartung[8], Pascale Hibon[8], Patrick Ingraham[5], Paul Kalas[4], Quinn Konopacky[2], Jérôme Maire[2], Franck Marchis[15], Mark S. Marley[16], Christian Marois[13], Max Millar-Blanchaer[2], Katie Morzinski[17,25], Andrew Norton[11], Rebecca Oppenheimer[18], David Palmer[6], Jennifer Patience[9], Marshall Perrin[19], Lisa Poyneer[6], Laurent Pueyo[19], Fredrik T. Rantakyrö[8], Naru Sadakuni[8], Leslie Saddlemyer[13], Dmitry Savransky[20], Andrew Serio[8], Anand Sivaramakrishnan[18,19], Inseok Song[21], Rémi Soummer[19], Sandrine Thomas[16], J. Kent Wallace[22], Sloane Wiktorowicz[23,25], and Schuyler Wolff[24]

[1] Department of Physics and Astronomy, University of California, Los Angeles, CA 90095, USA; jchilcote@astro.ucla.edu
[2] Dunlap Institute for Astronomy and Astrophysics University of Toronto, Toronto, Ontario M5S 3H4, Canada
[3] Lunar and Planetary Laboratory, University of Arizona, Tucson, AZ 85721, USA
[4] Astronomy Department, University of California, Berkeley, CA 94720, USA
[5] Kavli Institute for Particle Astrophysics and Cosmology, Stanford University, Stanford, CA 94305, USA
[6] Lawrence Livermore National Laboratory, Livermore, CA 94551, USA
[7] Department of Astrophysical Sciences, Princeton University, Princeton, NJ 08544, USA
[8] Gemini Observatory, Casilla 603, La Serena, Chile
[9] School of Earth and Space Exploration, Arizona State University, P.O. Box 871404, Tempe, AZ 85287, USA
[10] School of Physics, College of Engineering, Mathematics and Physical Sciences, University of Exeter, Stocker Road, Exeter EX4 4QL, UK
[11] University of California Observatories/Lick Observatory, University of California, Santa Cruz, CA 95064, USA
[12] Observatoire du Mont-M'egantic and D'epartement de physique Universit'e de Montr'eal, Montr'eal, QC H3T 1J4, Canada
[13] National Research Council of Canada Herzberg, 5071 West Saanich Road, Victoria, BC V9E 2E7, Canada
[14] Gemini Observatory, 670 North A'ohoku Place, Hilo, HI 96720, USA
[15] SETI Institute, Carl Sagan Center, 189 Bernardo Avenue, Mountain View, CA 94043, USA
[16] NASA Ames Research Center, Mountain View, CA 94035, USA
[17] Steward Observatory, University of Arizona, Tucson, AZ 85721, USA
[18] Department of Astrophysics, American Museum of Natural History, New York, NY 10024, USA
[19] Space Telescope Science Institute, Baltimore, MD 21218, USA
[20] Sibley School of Mechanical and Aerospace Engineering, Cornell University, Ithaca, NY 14853, USA
[21] Department of Physics and Astronomy, University of Georgia, Athens, GA 30602, USA
[22] Jet Propulsion Laboratory, California Institute of Technology, Pasadena, CA 91125, USA
[23] Department of Astronomy, University of California—Santa Cruz, 1156 High Street, Santa Cruz, CA 95064, USA
[24] Department of Physics and Astronomy, Johns Hopkins University, Baltimore, MD 21218, USA
Received 2014 July 15; accepted 2014 November 6; published 2014 December 12

ABSTRACT

Using the recently installed Gemini Planet Imager (GPI), we have obtained the first *H*-band spectrum of the planetary companion to the nearby young star β Pictoris. GPI is designed to image and provide low-resolution spectra of Jupiter-sized, self-luminous planetary companions around young nearby stars. These observations were taken covering the *H* band (1.65 μm). The spectrum has a resolving power of ~45 and demonstrates the distinctive triangular shape of a cool substellar object with low surface gravity. Using atmospheric models, we find an effective temperature of 1600–1700 K and a surface gravity of $\log(g) = 3.5$–4.5 (cgs units). These values agree well with "hot-start" predictions from planetary evolution models for a gas giant with mass between 10 and 12 $M_{\rm Jup}$ and age between 10 and 20 Myr.

Key words: infrared: general – instrumentation: adaptive optics – planetary systems – stars: individual (beta Pictoris) – techniques: spectroscopic

1. INTRODUCTION

For over a decade, there have been ongoing efforts to directly image young Jupiter-mass exoplanets still luminous in the infrared (IR) from their formation process. Examples of such planets include 2M1207b (Chauvin et al. 2005), Fomalhaut b (Kalas et al. 2008), the HR8799 system (Marois et al. 2008, 2010), β Pictoris (Pic) b (Lagrange et al. 2010), IRXS J1609 b (Lafrenière et al. 2010), HD 95086 b (Rameau et al. 2013), and GJ 504 b (Kuzuhara et al. 2013).

Beta Pictoris (HD 39060) is a 21 ± 4 Myr (Binks & Jefferies 2014), A6V star located 19.44 ± 0.05 pc from Earth (Gray et al. 2006; van Leeuwen 2007). β Pic represents the earliest example of high-contrast imaging to directly detect a circumstellar disk (Smith & Terrile 1984). The disk is viewed edge-on and shows asymmetric structure that has been attributed to planetary perturbations (Burrows et al. 1995; Kalas & Jewitt 1995; Golimowski et al. 2006; Mouillet et al. 1997; Heap et al. 2000; Augereau et al. 2001). The planet possibly responsible for these perturbations was discovered by direct imaging (Lagrange et al. 2010). β Pic b has been detected by Very Large Telescope (VLT)/NACO (Lagrange et al. 2010), Gemini/NICI (Boccaletti et al. 2013), Magellan adaptive optics (AO; Males

[25] NASA Sagan Fellow.

et al. 2014; Morzinski et al. 2014), and Gemini/GPI (Macintosh et al. 2014). In the H band, β Pic b has an absolute magnitude of $H_{\rm MKO} = 11.87 \pm 0.11$. The basic properties of β Pic b have been estimated using spectral energy distribution fitting of broadband photometry, resulting in an effective temperature of 1700 ± 100 K with a $\log g = 4.0 \pm 0.5$ (Bonnefoy et al. 2013). Previous comparisons of the planet's bolometric luminosity and system age to evolutionary "hot-start" cooling tracks resulted in a mass from 9 to 13 $M_{\rm Jup}$ (Bonnefoy et al. 2013; Males et al. 2014). Using a cross-correlation technique and high spectral resolution over a narrow wavelength range, Snellen et al. (2014) were able to measure the planet's spin ($v \sin(i) \sim 25$ km s^{-1}) and detect carbon monoxide absorption in the K band.

Understanding the atmospheres of these very young giant exoplanets is a challenging task because we only have a handful of objects to study spectroscopically. The theoretical models used to compute the emergent flux from these planetary atmospheres are often extensions of those generated for brown dwarfs, yet the spectra of the HR8799 planets exhibit significant differences relative to brown dwarfs (Barman et al. 2011a; Marley et al. 2012). Spectroscopy of β Pic b offers another opportunity to study the atmospheric properties of a young giant planet that is substantially hotter than the HR8799 planets.

We present the first H-band spectral mode observations of β Pic b with the Gemini Planet Imager (GPI). An analysis of the orbital parameters using astrometric measurements from GPI is published in Macintosh et al. (2014). In Section 2, we discuss observations with the recently delivered GPI and data reduction used to analyze the spectrum with this new instrument. Analysis of the H-band spectrum, along with existing photometry, is presented in Section 3. Conclusions are discussed in Section 4.

2. OBSERVATIONS AND DATA REDUCTION

GPI was designed and built to directly image and spectroscopically characterize young, Jupiter-sized, self-luminous extrasolar planets (Macintosh et al. 2006; Graham et al. 2007). GPI was installed at Gemini South in the fall of 2013. GPI first light and commissioning tests demonstrate that the AO system lowers the total wavefront error from dynamic sources and quasi-static errors by an order of magnitude compared to earlier AO systems (Macintosh et al. 2014; Poyneer et al. 2014). Diffraction is suppressed by an apodized-pupil Lyot coronagraph (Soummer et al. 2011; Macintosh et al. 2014). The science instrument is a near-IR (1–2.5 μm) integral field spectrograph (IFS; Chilcote et al. 2012; Larkin et al. 2014). The spatial field is sampled by a lenslet array and then dispersed, resulting in ~37,000 individual spectra with a spectral resolving power of $R = \lambda/\delta\lambda \sim 30$–$90$. The spatial plane is sampled at 14.14 ± 0.01 mas pixel^{-1} (Konopacky et al. 2014). In first light observations, GPI achieved a 5σ contrast of 10^5 at 0.″35 and 10^6 at 0.″75 (Macintosh et al. 2014).

β Pic was observed with GPI in the H band (1.5072 μm–1.7899 μm,[26] $R \sim 44$–49) by the GPI Verification and Commissioning team on 2013 November 18 and 2013 December 10, respectively. During November observations, 32 individual 59.6 s images were obtained in coronagraphic mode, with the cryocoolers (Chilcote et al. 2012; Larkin et al. 2014) operating at a reduced power level to reduce the effects of vibration introduced into the telescope. Seeing conditions were on average 0.″68 as measured by the Gemini South DIMM. As the observations were performed during instrument commissioning, various operational modes were used during a specific data set to evaluate the performance of the instrument. During the 2013 December observations, 14 individual 59.6 s images were obtained in coronagraphic mode. For eight of the images, the IFS cryocoolers were operating at full power, while in the remaining six images, the cryocoolers were operating in a reduced power state similar to the November observations. Each image has a different spatial filter size and woofer integrator memory value in an attempt to optimize AO performance (Macintosh et al. 2014). Immediately after the observing sequence was completed, and at the same telescope orientation and flexure, a single observation of the flood-illuminated argon calibration source was taken to accurately track the shift of the spectral solution on the HAWAII-2RG detector.

The images were first processed using the GPI data reduction pipeline (Perrin et al. 2014). The pipeline requires the location and spectral solution for every lenslet. These lenslet locations were determined by using a cross correlation of the single argon image taken during the observing sequence as β Pic and high signal-to-noise ratio (S/N), deep images made during daytime calibrations. The telescope elevation differed between the science images and the daytime calibration sequence. The resultant shift was used to determine the overall change of the wavelength solution between the daytime calibrations and that appropriate for the observations of β Pic.

With a shifted wavelength calibration, the GPI data reduction pipeline was used to reduce all images, apply dark corrections, remove bad pixels, track satellite spot locations, and convert each microspectra into a 37 channel spectral cube (1.490–1.802 μm). Each data set was processed in an identical way.

Further data processing was done outside of the GPI pipeline. The GPI atmospheric dispersion corrector was not commissioned at the time these observations were made; therefore, each image and each spectral slice are independently registered using the stellar position found by the four satellite spots. GPI is mounted on a Cassegrain port with derotator disabled so each image has a different sky orientation. Due to imaging constraints, neither angular nor spectral differential imaging were performed. In post processing, these images are rotated so that the planet has a fixed location.

Since the satellite spots are imaged at an identical time under identical conditions, in theory, their point-spread functions (PSFs) should closely match the planet PSF especially when the four spots are averaged together. Instrumental effects and atmospheric effects are estimated from satellite spot spectra. An 8000 K, $\log g = 4.0$ (Gray et al. 2006) BT–Nexgen model (Allard et al. 2012) convolved to the resolution of GPI was used to approximate the A6V stellar spectrum of β Pic A. This allows the instrumental and telluric features under identical conditions to be estimated for the planet spectrum and removed.

We found that the remaining halo in these initial first light images was smooth, and dominated by uncorrected atmospheric halo speckles rather than quasi-static speckles. In order to remove this halo, we fit a third-order spline surface to an annulus of radius = 57.2–114.4 mas centered on the location of the planet, which includes the space around the planet but does not include the planet itself. A PSF, generated by the average of the four satellite spot cores, was scaled and subtracted from the planet position in parallel to the spline fit. This average PSF of the four satellite spots was generated for each particular image and wavelength channel to which it corresponds. This spline surface + reference PSF is generated to subtract the smooth halo and estimate the flux of the PSF. A Levenberg–Marquardt

[26] Defined by the 80% power point of the filters.

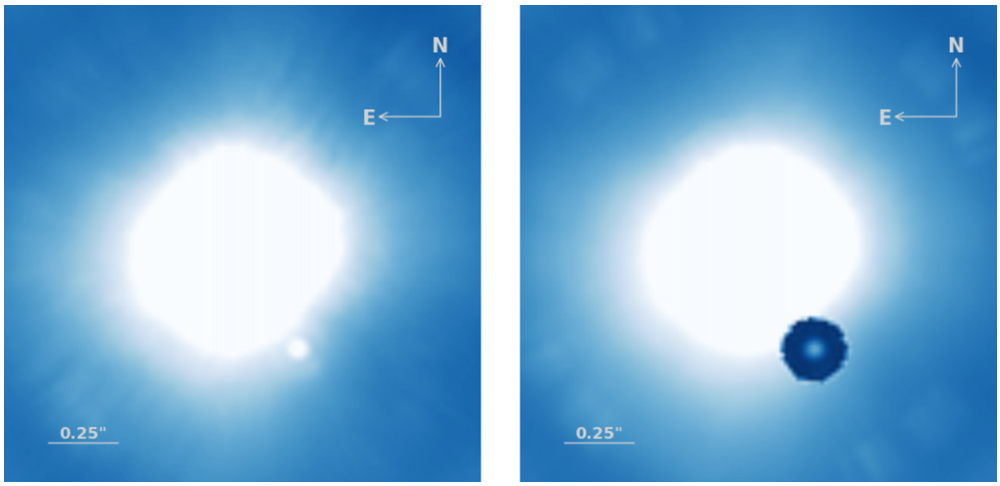

Figure 1. Left: average image of β Pic b from 2013 November with no post-processing removal of the background. Right: left image with a circular annulus defined around the estimated location of the planet, which has been used to define a surface in each image and spectral channel to subtract the remaining halo light. In order to remove this halo, we fit a third-order spline surface to an aperture of radius = 57.2–114.4 mas centered on the location of the planet, which includes the space around the planet but does not include the planet itself. A PSF, generated by the average of the four satellite spot cores, was scaled and subtracted from the planet position in parallel to the spline fit.

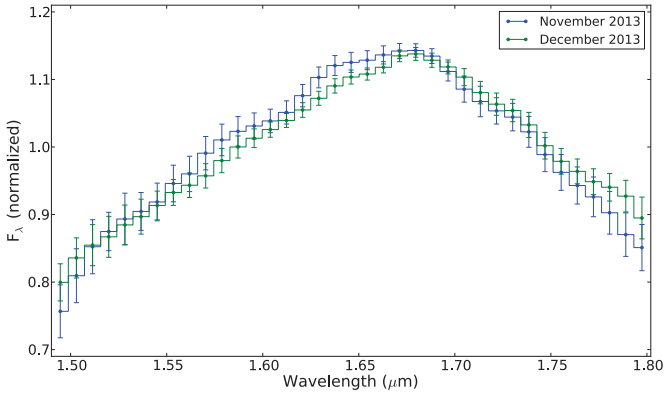

Figure 2. 2013 November and December H-band spectra of β Pic b using GPI. Both spectra are in agreement. The spectra were taken at different phases of the GPI commissioning process resulting in different effects on the light in the halo and PSF shape.

least-squares minimization (Markwardt 2009) was performed to find the best fit of the underlying halo and the planet PSF in each image and at each spectral channel (Figure 1). We performed this two component fit because the wings of the PSF influence the spline fit. By fitting both simultaneously, we remove the impact of the PSF wings on the spline surface.

We determined the spectrum using the flux of the PSF component of the background subtraction technique of the spline fit + PSF to measure the flux from the injected reference PSF. This produces measurements of the planet's flux in each spectral channel. For robustness, we compared this value against aperture photometry of the planet and measured nearly the same value, but with slightly higher errors. Each of the individual spectra measured from the individual frames is independently normalized and combined together (Figure 2). To estimate the systematic errors and residuals, PSFs were generated from the satellite spots, injected with a flat spectrum at an identical radius from the host star into the individual frames, and then reduced in an identical manner. Given that this is one of the first extracted spectrum from the new GPI instrument, and that the halo of the star has significant color variation, it is possible that the overall spectral slope has an uncertainty of approximately 10% that is not included in our error analysis.

3. RESULTS AND DISCUSSION

The spectrum discussed above has a S/N per wavelength channel that matches or exceeds most previous broadband photometry with an average S/N $\sim$ 61. With this spectrum, we can estimate surface gravity and effective temperature as well as search for molecular absorption features and departures from stellar abundances.

The H-band spectrum has a clear peak at 1.68 μm defined by absorption on either side. The location of this peak and the slopes on either side are consistent with water absorption frequently seen in brown dwarf spectra. Based on previous photometric estimates of the effective temperature, the primary opacity sources across the near-IR are water, collision-induced absorption from H_2, and dust. There is no evidence for additional molecular absorption (e.g., from methane or ammonia). The H-band spectrum has a very triangular shape, a hallmark of low surface gravity and further evidence of β Pic b's low mass and youth.

The GPI H-band spectrum and existing ground-based photometry were compared to the model grids described in Barman et al. (2011a, 2011b). An effective temperature of 1600–1700 K was found to best match these spectral data, in excellent agreement with previous photometric studies (Bonnefoy et al. 2013; Currie et al. 2013; Males et al. 2014). The best matching model is shown in Figure 3 and it agrees well with the visible to IR photometry (Figure 4). Broadband photometric colors, however, are only modestly sensitive to surface gravity, emphasizing the need for spectral data. Our H-band spectrum, as previously discussed, has a triangular shape that sensitively depends on surface gravity. Our best matching models have $\log(g) = 3.5$–4.5 (cgs units) that, when taken into consideration along with the effective temperature of 1650 K, is consistent with evolutionary models between 10 and 20 Myr for masses between 10 and 12 $M_{\rm Jup}$ (Burrows et al. 1997; Chabrier et al. 2000).

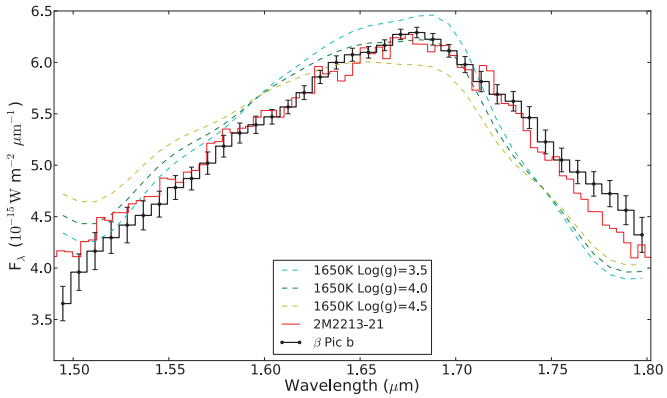

Figure 3. Comparison of the *H*-band spectrum (black) to a 1650 K model with three different gravities. All three models do not provide a perfect match to the spectrum. The $\log(g) = 4.0$ model (green) comparison has the best fit but is offset from the observations by a constant slope. The young, low-gravity brown dwarf 2M2213-21 (red) has a better match to the spectrum than all three models. The agreement between the GPI spectrum and that of known low-gravity brown dwarfs strongly suggests that our GPI spectrum is mostly free of chromatic systematic errors and the discrepancies with the synthetic spectra are most likely the result of imperfect modeling (e.g., treatment of dust clouds). The spectra are normalized to match the flux measured in Males et al. (2014).

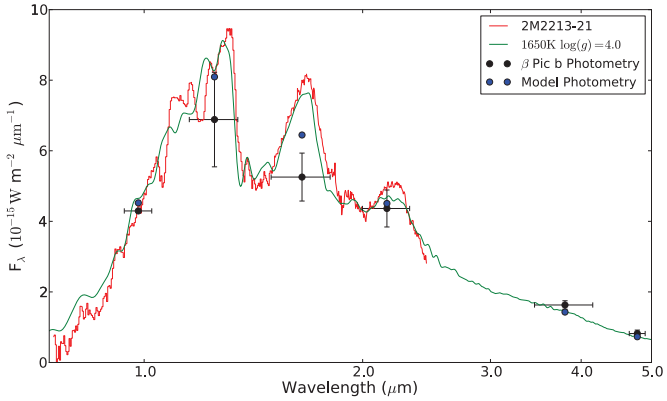

Figure 4. We compare the model 1650 K $\log(g) = 4.0$ spectrum (green) and its predicted photometric points (blue) to the spectrum of 2M2213-21 (red) and the measured photometric points of β Pic b (black) (e.g., Males et al. 2014, and references therein).

Comparing the spectrum to BT-Settl and BT-Dusty models (Allard et al. 2012) resulted in a higher gravity, $\log(g) = 5.0$, highlighting the model-dependent nature of our best matching gravity range. As suggested by others, BD model atmospheres have lingering systematic offsets when compared to observations. Therefore, we stress that our reported gravity range is model dependent, and hence subject to possible systematic offsets. At high gravities, however, it is not supported by the empirical comparisons made using the low-gravity standards from Allers & Liu (2013) and their *H*-band gravity index.

Figure 5 compares the GPI β Pic b spectrum to those of other directly imaged planetary-mass companions and field objects: 2M0437 (Bowler et al. 2014), SIMP J215434.5−105530.8 (Gagné et al. 2014a), 2MASS J12074836−3900043 (Gagné et al. 2014b), AB Pic b (Bonnefoy et al. 2014), 2M1207 b (Patience et al. 2010), and HR8799 b (Barman et al. 2011a) and HR8799 c (Oppenheimer et al. 2013). All of these objects are reported to exhibit low gravity. The HR8799 planets shown

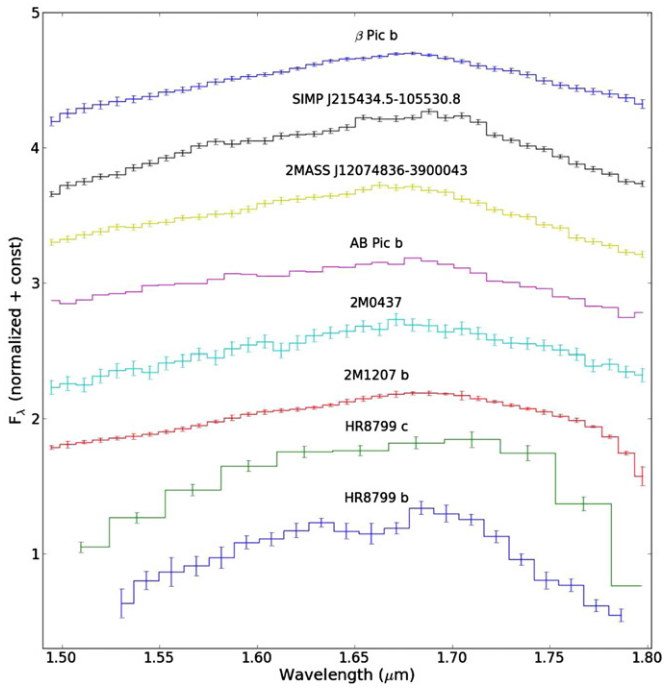

Figure 5. *H*-band spectra of young, directly imaged planets. The Gemini Planet Imager spectrum of β Pic b is plotted above the spectra of 2M0437 (Bowler et al. 2014), SIMP J215434.5−105530.8 (Gagné et al. 2014a), 2MASS J12074836−3900043 (Gagné et al. 2014b), AB Pic b (Bonnefoy et al. 2014), 2M1207b (Patience et al. 2010), and HR8799 c (Oppenheimer et al. 2013) and b (Barman et al. 2011a). Each of these objects is cooler than β Pic b. Despite very different temperatures, 2M0437, 2M1207b, 2MASS J12074836−3900043, and β Pic b have atmospheres with similar dominant opacity sources. The differences between β Pic b and HR8799 b and c highlights the spectral evolution of low-gravity objects.

in Figure 5 are all cooler than β Pic b by ∼500–800 K. Despite temperature differences, 2M1207b and β Pic b have similar *H*-band spectra. 2M1207b's *H*-band spectrum is shaped by a combination of low gravity, opacity from thick dusty clouds, and non-equilibrium chemistry that favors CO over methane (Barman et al. 2011b). Non-equilibrium chemistry is less important in hotter objects like β Pic b that will have a large CO/CH_4 ratio, regardless of vertical mixing. Consequently, despite very different temperatures, 2M0437, 2M1207b, and β Pic b have atmospheres with similar dominant opacity sources. The *H*-band similarities between these objects supports the idea that β Pic b is low gravity (and hence low mass) and clouds 1–2 pressure scale heights near the photosphere. The differences between β Pic b and HR8799 b and c seen in Figure 5 highlight the spectral evolution of low-gravity objects from high to low effective temperatures.

The model spectra (Figure 3), however, do not match the *H*-band spectrum particularly well. The best matching model under-predicts the fluxes at $\lambda > 1.7$ μm while slightly over-predicting the fluxes on the blue side of the *H*-band peak. The net effect is a systematic tilt of 5%–10% between the model and the data. Though a spectral offset of this magnitude may be present in the data, we found that most *H*-band spectra from a low-gravity brown dwarf spectral sequence (Allers & Liu 2013) agree extremely well with our GPI spectrum. The best matching brown dwarf, 2M2213-21, has a reduced $\chi^2 = 1.7$ (see Figure 5) and the red-optical through *K*-band spectrum of 2M2213-21 also closely follows the β Pic b photometry. Like β

Pic b, 2M2213-21 is a young object with low-gravity features and a possible member of the β Pic moving group, at the $\sim$30% level (Manjavacas et al. 2014). In comparison to Allers & Liu (2013), β Pic b falls among the low-gravity dwarfs and far from the field dwarfs. The agreement between the GPI spectrum and that of known low-gravity brown dwarfs strongly suggests that our GPI spectrum is mostly free of chromatic systematic errors and the discrepancies with the synthetic spectra are most likely the result of imperfect modeling (e.g., treatment of dust clouds). Such a systematic discrepancy in the model spectra could bias the derived surface gravity, but it is unclear by how much. Allowing for a slight $\pm$10% tilt in the model H-band spectra yields much improved fits, but does not notably change the resulting surface gravity.

4. CONCLUSION

Using data from the recently commissioned GPI, we present the first H-band spectrum of the extrasolar planet β Pic b. We find that the spectrum of β Pic b provides a new and insightful look at the atmospheres of these high-temperature, low-gravity objects. While the best matching model does not perfectly match the H-band spectrum, the spectrum is remarkably similar to the young, low-gravity brown dwarf 2M2213-21. We thus conclude that error most likely is derived from imperfect modeling of the atmosphere. With so few directly imaged planet spectra, the other known objects are estimated to be cooler than β Pic b, and have a slightly different spectral shape.

Currently, and in the near future, several extreme-AO instruments (GPI/Gemini (Macintosh et al. 2014), SCExAO/Subaru (Guyon et al. 2010), SPHERE/VLT Beuzit et al. (2008)) will be online with the capability to directly image the spectra of the extrasolar planets they find. While our β Pic b data only cover the H band, GPI is designed to measure spectra from 0.95 to 2.4 μm with a capability similar to our H-band data. These spectra will further our understanding of these high-temperature, low-gravity objects. The low resolution but great sensitivity of GPI is well designed to identify and characterize low-gravity young exoplanets, as is demonstrated in our β Pic b spectrum.

The authors acknowledge the financial support of the Gemini Observatory, the NSF Center for Adaptive Optics at UC Santa Cruz, the NSF (AST-0909188; AST-1211562, AST-1405505), NASA Origins (NNX11AD21G; NNX10AH31G, NNX14AC21G), the University of California Office of the President (LFRP-118057), the Science and Technology Facilities Council (ST/H002707/1), and the Dunlap Institute, University of Toronto. Portions of this work were performed under the auspices of the U.S. Department of Energy by Lawrence Livermore National Laboratory under Contract DE-AC52-07NA27344 and under contract with the California Institute of Technology/Jet Propulsion Laboratory funded by NASA through the Sagan Fellowship Program executed by the NASA Exoplanet Science Institute. We are indebted to the international team of engineers and scientists who worked to make GPI a reality.

Facility: Gemini:South (GPI)

REFERENCES

Allard, F., Homeier, D., & Freytag, B. 2012, RSPTA, 370, 2765
Allers, K. N., & Liu, M. C. 2013, ApJ, 772, 79
Augereau, J. C., Nelson, R. P., Lagrange, A. M., Papaloizou, J. C. B., & Mouillet, D. 2001, A&A, 370, 447
Barman, T. S., Macintosh, B., Konopacky, Q. M., & Marois, C. 2011a, ApJ, 733, 65
Barman, T. S., Macintosh, B., Konopacky, Q. M., & Marois, C. 2011b, ApJL, 735, L39
Beuzit, J.-L., Feldt, M., Dohlen, K., et al. 2008, Proc. SPIE, 7014, 701418
Binks, A. S., & Jeffries, R. D. 2014, MNRAS, 438, L11
Boccaletti, A., Lagrange, A.-M., Bonnefoy, M., Galicher, R., & Chauvin, G. 2013, A&A, 551, L14
Bonnefoy, M., Boccaletti, A., Lagrange, A.-M., et al. 2013, A&A, 555, A107
Bonnefoy, M., Chauvin, G., Lagrange, A.-M., et al. 2014, A&A, 562, A127
Bowler, B. P., Liu, M. C., Kraus, A. L., & Mann, A. W. 2014, ApJ, 784, 65
Burrows, A., Marley, M., Hubbard, W. B., et al. 1997, ApJ, 491, 856
Burrows, C. J., Krist, J. E., Stapelfeldt, K. R., & WFPC2 Investigation Definition Team., 1995, BAAS, 27, 1329
Chabrier, G., Baraffe, I., Allard, F., & Hauschildt, P. 2000, ApJ, 542, 464
Chauvin, G., Lagrange, A.-M., Dumas, C., et al. 2005, A&A, 438, L25
Chilcote, J. K., Larkin, J. E., Maire, J., et al. 2012, Proc. SPIE, 8446, 84468W
Currie, T., Burrows, A., Madhusudhan, N., et al. 2013, ApJ, 776, 15
Gagné, J., Faherty, J. K., Cruz, K., et al. 2014a, ApJL, 785, L14
Gagné, J., Lafrenière, D., Doyon, R., et al. 2014b, ApJL, 792, L17
Golimowski, D. A., Ardila, D. R., Krist, J. E., et al. 2006, AJ, 131, 3109
Graham, J. R., Macintosh, B., Doyon, R., et al. 2007, arXiv:0704.1454
Gray, R. O., Corbally, C. J., Garrison, R. F., et al. 2006, AJ, 132, 161
Guyon, O., Martinache, F., Garrel, V., et al. 2010, Proc. SPIE, 7736, 773624
Heap, S. R., Lindler, D. J., Lanz, T. M., et al. 2000, ApJ, 539, 435
Kalas, P., Graham, J. R., Chiang, E., et al. 2008, Sci, 322, 1345
Kalas, P., & Jewitt, D. 1995, AJ, 110, 794
Konopacky, Q. M., Thomas, S. J., Macintosh, B. A., et al. 2014, Proc. SPIE, 9147, 914784
Kuzuhara, M., Tamura, M., Kudo, T., et al. 2013, ApJ, 774, 11
Lafrenière, D., Jayawardhana, R., & van Kerkwijk, M. H. 2010, ApJ, 719, 497
Lagrange, A.-M., Bonnefoy, M., Chauvin, G., et al. 2010, Sci, 329, 57
Larkin, J. E., Chilcote, J. K., Aliado, T., et al. 2014, Proc. SPIE, 9147, 91471K
Macintosh, B., Graham, J., Palmer, D., et al. 2006, Proc. SPIE, 6272, 62720L
Macintosh, B., Graham, J. R., Ingraham, P., et al. 2014, PNAS, 111, 12661
Males, J. R., Close, L. M., Morzinski, K. M., et al. 2014, ApJ, 786, 32
Manjavacas, E., Bonnefoy, M., Schlieder, J. E., et al. 2014, A&A, 564, A55
Markwardt, C. B. 2009, in ASP Conf. Ser. 411, Astronomical Data Analysis Software and Systems XVIII, ed. D. A. Bohlender, D. Durand, & P. Dowler (San Francisco, CA: ASP), 251
Marley, M. S., Saumon, D., Cushing, M., et al. 2012, ApJ, 754, 135
Marois, C., Macintosh, B., Barman, T., et al. 2008, Sci, 322, 1348
Marois, C., Zuckerman, B., Konopacky, Q. M., Macintosh, B., & Barman, T. 2010, Natur, 468, 1080
Morzinski, K. M., Close, L. M., Males, J. R., et al. 2014, in IAU Symp. 299, Exploring the Formation and Evolution of Planetary Systems, ed. M. Booth, B. C. Matthews, & J. R. Graham (Cambridge: Cambridge Univ. Press), 252
Mouillet, D., Larwood, J. D., Papaloizou, J. C. B., & Lagrange, A. M. 1997, MNRAS, 292, 896
Oppenheimer, B. R., Baranec, C., Beichman, C., et al. 2013, ApJ, 768, 24
Patience, J., King, R. R., de Rosa, R. J., & Marois, C. 2010, A&A, 517, A76
Perrin, M., Maire, J., Ingraham, P. J., et al. 2014, Proc. SPIE, 9147, 91473J
Poyneer, L. A., De Rosa, R. J., Macintosh, B., et al. 2014, Proc. SPIE, 9148, 91480K
Rameau, J., Chauvin, G., Lagrange, A.-M., et al. 2013, ApJL, 772, L15
Smith, B. A., & Terrile, R. J. 1984, Sci, 226, 1421
Snellen, I. A. G., Brandl, B. R., de Kok, R. J., et al. 2014, Natur, 509, 63
Soummer, R., Sivaramakrishnan, A., Pueyo, L., Macintosh, B., & Oppenheimer, B. R. 2011, ApJ, 729, 144
van Leeuwen, F. 2007, A&A, 474, 653